Zeitschrift für Physikalische Chemie, **214**, 8, 1035–1063 (2000)

Collision-Induced Dissociation Dynamics of the $[OCS \cdot C_2H_2]^+$ Complex. A Combined Experimental and Theoretical Study

By Felician Muntean and P. B. Armentrout*

Chemistry Department, University of Utah, Salt Lake City, UT 84112, USA

Dedicated to Prof. Dr. Dr. h. c. mult. Jürgen Troe on the occasion of his 60th birthday

(Received March 30, 2000; accepted May 2, 2000)

Collision-Induced Dissociation / Competitive Shift / Ethylene Sulfide Cation / Kinetic Shift / Thioketene Cation

Collision-induced dissociation (CID) of the $[OCS \cdot C_2H_2]^+$ complex ion with both Xe and Ar over an energy range of 0 to 10 eV in the center of mass frame is studied using a guided ion beam tandem mass spectrometer. The cross sections of the ionic products observed ($C_2H_2S^+$, OCS^+, $C_2H_2^+$, and S^+) are analyzed by taking into account reactant energy distributions, multiple collisions, lifetime effects and competition. A recently devised statistical model for the simultaneous analysis of competitive product channels is used to analyze three channels for the first time, with good results. Thresholds for product formation at 0 Kelvin are 0.33 ± 0.07 eV for $C_2H_2S^+$, 0.95 ± 0.07 eV for OCS^+, 1.22 ± 0.08 eV for $C_2H_2^+$, and an upper limit of 4.26 eV for S^+. These results are comparable to available literature thermochemical data within experimental errors. Competitive shifts are significant, about 0.3 eV for both OCS^+ and $C_2H_2^+$. *Ab initio* calculations at the QCISD/6-311+G**//MP2/6-311+G** and CCSD//6-31G*//CCD/6-31G* levels are performed on the system. The reaction coordinates of the potential energy surface of the system is quantitatively mapped using results from CID and *ab initio* calculations. The identity of the $C_2H_2S^+$ product is suggested to be the cyclic ethylene sulfide cation on the basis of the results of calculations and previous kinetic energy release measurements. Product branching ratios as a function of energy are analyzed and compared to those determined in previous photodissociation and bimolecular reaction experiments.

1. Introduction

The $[OCS \cdot C_2H_2]^+$ system is a good case for studying the difficult dynamics of polyatomic molecule reactions. It presents all the main characteristics of polyatomic systems (multidimensional potential energy surfaces, multiple

* Corresponding author.

isomers, multiple types of transition states leading to several product channels, and complex lifetime effects) while being small enough to enable extensive experimental and theoretical investigations.

The first study on this system was reported by Anderson and coworkers [1, 2], who examined ion-molecule reactions (1)–(4) in a guided ion beam tandem mass spectrometer.

$$C_2H_2^+ + OCS \rightarrow C_2H_2S^+ + CO \quad (1)$$

$$\rightarrow OCS^+ + C_2H_2 \quad (2)$$

$$OCS^+ + C_2H_2 \rightarrow C_2H_2S^+ + CO \quad (3)$$

$$\rightarrow C_2H_2^+ + OCS \quad (4)$$

The major product channels are the result of sulfur atom transfer, reactions (1) and (3), exothermic in both systems. The other major process is charge transfer, slightly exothermic in reaction (2) and endothermic in reaction (4). Using resonance-enhanced multiphoton ionization (REMPI), Anderson and coworkers formed vibrationally state-selected reactant ions and studied how the reaction cross sections varied with excitation of different modes.

Inspired by the fact that the dynamics of these reactions implied the occurrence of a long lived collision complex, Orlando *et al.* [3] formed the $[OCS \cdot C_2H_2]^+$ complex in a high pressure ion source and studied it by photodissociation (PD) spectroscopy. In the 375–735 nm range, they observed OCS^+, $C_2H_2^+$, and $C_2H_2S^+$ as the main products. They concluded that the PD dynamics involves an excited potential energy surface (PES) of the system and provided an upper limit of 1.46 eV for the complex bond dissociation energy with respect to the OCS^+ product. Considering the thermal energy content of the complex, they also suggested the existence of a reverse barrier of at least 0.15 eV to the $C_2H_2S^+$ product channel.

Another study that improved the characterization of the system was reported by Graul and Bowers [4]. They formed the complex in a cooled, high pressure electron ionization source and performed mass-analyzed ion kinetic energy spectrometry (MIKES), PD spectroscopy experiments, and *ab initio* calculations on the system. They analyzed kinetic energy release distributions (KERDs) of the products and were able to set the main qualitative features of the PES: a reverse barrier in the $C_2H_2S^+$ product channel and barrierless transitions to the $C_2H_2^+$ and OCS^+ product channels. PD results were explained by excitations to repulsive excited states. Geometries and energies of all product channels were calculated at the MP2/6-31+G* level. Three stable isomers for the $C_2H_2S^+$ product were found, although only the thioketene (the most stable) and the cyclic ethylene sulfide structures were thermodynamically consistent with the experimental results. For the $[OCS \cdot C_2H_2]^+$ complex, theoretical calculations at the HF/6-31+G* level revealed a structure for the complex ion with near σ-bonding between the S atom of OCS and one of the C atoms of C_2H_2.

Finally, Chiu *et al.* [5] reported mode-selective, differential cross section measurements on the bimolecular reactions (1)–(4), revealing additional mechanistic information on the system. They found that S atom transfer occurs by similar mechanisms in both reactions: complex-mediated at very low energies and direct (rebound and stripping) at higher energies. The two charge transfer reactions proceed through different mechanisms: long range electron hopping for the exothermic reaction (2) and one that involves impulsive collisions for the endothermic reaction (4).

In the present paper, we present results of a collision-induced dissociation (CID) experiment in the energy range of 0 to 10 eV center of mass and higher level *ab initio* calculations on the $[OCS \cdot C_2H_2]^+$ system. The CID thresholds provide the height of the activation barrier for sulfur transfer, the depth of the $[OCS \cdot C_2H_2]^+$ potential well, and other values needed to complete a quantitative characterization of the PES. The analysis of CID product branching ratios as a function of energy reveals additional mechanistic information by comparison to previous PD and bimolecular reaction branching ratios. The calculations provide optimized structures for the complex ion and products, vibrational frequencies and rotational constants used in the analysis of the experimental data, and energetic details of the PES.

2. Experimental and computational section

General experimental procedures

CID experiments were performed on a guided ion beam tandem mass spectrometer, which has been previously described in detail [6, 7]. Briefly, the ion source used in this experiment consists of a microwave discharge followed by a one meter long flow tube [8]. He gas is introduced in the ion source and ionized by the discharge, OCS gas is introduced in the flow tube about 10 cm from the ion source and C_2H_2 gas is introduced downstream, about 50 cm from the ion source. OCS^+ ions are formed by charge transfer from He ions and possibly by Penning ionization. $[OCS \cdot C_2H_2]^+$ ions are formed by three-body stabilization of OCS^+ and C_2H_2 in the He atmosphere (about 0.7 Torr), then thermalized by many collisions ($>10^4$) with He in the flow. We assume that the complex ions are in their ground electronic state, with an internal energy distribution well characterized by a Maxwell-Boltzmann distribution of ro-vibrational states at room temperature. This assumption is supported by many years of experimental evidence in our laboratory [9–12].

Complex ions are sampled from the flow tube, focused through two regions of differential pumping, mass selected by a magnetic analyzer, and injected with the desired energy into the rf octopole ion beam guide. The guide passes through the collision cell, where CID occurs. We performed experiments with both Xe and Ar as collision gases, at cell pressures typi-

cally between 0.05 and 0.20 mTorr. The cross sections showed no dependence on pressure over this range, demonstrating that single collision conditions were met. Primary ions and collision products drift to the end of the octopole, where they are extracted, mass selected by a quadrupole analyzer, and detected by a secondary electron scintillation detector. Ion intensities are measured using standard counting electronics.

Measuring ion intensities are converted to cross sections, as described previously [6]. Laboratory ion energies are calibrated using a retarding analysis in the octopole guide [6]. The distributions showed a Gaussian shape with a typical FWHM around 0.2 eV. Uncertainties are estimated to be ±20% for the absolute cross sections and ±0.05 eV for laboratory frame energies. Laboratory energies are converted to center-of-mass (CM) energies using the stationary target approximation, as previously described [6]. All energies mentioned in this paper refer to the CM frame, unless otherwise specified.

Data analysis

CID product cross sections as a function of collision energy are modeled using a modified line-of-centers model [8, 12], Eq. (5)

$$\sigma(E) = \sigma_0 \sum_i g_i(E + E_i - E_0)^n / E \tag{5}$$

where σ is the cross section, E is the collision energy, E_0 is the reaction threshold at 0 K, σ_0 and n are adjustable parameters, and the summation is over ro-vibrational states of the reactant ion having energies E_i with populations g_i. The necessary vibrational frequencies and rotational constants are obtained from the *ab initio* calculations described below. The Beyer-Swinehart algorithm [13, 14] is used to calculate the density of ro-vibrational states and the relative populations are calculated by a Maxwell-Boltzmann distribution at the appropriate temperature of the reactants. Eq. (5) is further convoluted over the kinetic energy distributions of the two reactants: experimentally determined for the primary ion and Maxwell-Boltzmann for the neutral gas, as previously described [6].

In cases where dissociation is slow compared to the time of flight of the dissociating molecule through the instrument, products are not efficiently observed until energies higher than the real dissociation threshold, yielding what is called a kinetic shift or lifetime effect. No matter how good the experimental sensitivity, there is a minimum rate of product formation necessary to enable detection above background noise. To include lifetime effects in our data analysis, we follow the procedure described in detail previously [15, 16]. Briefly, we use Eq. (6), in which our CID model (5) is complemented with a integration over a unimolecular dissociation probability.

$$\sigma(E) = (n\sigma_0/E) \sum_i g_i \int_0^{E+E_i-E_0} [1 - e^{-k(E+E_i-\Delta E)\tau}](\Delta E)^{n-1} d(\Delta E) \quad (6)$$

Here, ΔE is the residual kinetic energy (the energy which remains in translation after collision), τ is the experimental time available for dissociation (the ion time of flight from the collision cell to the quadrupole mass analyzer, approximately 10^{-4} s), and $k(E + E_i - \Delta E) = k(E^*)$ is the unimolecular dissociation rate constant, calculated using RRKM theory [17–19]. In the limit that $k(E^*)$ is faster than the time-of-flight of the ions, this integration recovers Eq. (5).

In cases in which two or more product channels are in competition to one another, the formation of higher energy products can be inhibited, such that their detection may only be possible at energies that are higher than the real thresholds. This leads to what are usually called competitive shifts. To account for such competition, we use the model recently derived and discussed in a previous paper [20]. Briefly, the equation used to model our CID data in this case is

$$\sigma_j(E) = \frac{n\sigma_{0,j}}{E} \sum_i g_i \int_0^{E+E_i-E_0} \frac{k_j(E^*)}{k_{tot}(E^*)} [1 - e^{-k_{tot}(E^*)\tau}](\Delta E)^{n-1} d(\Delta E), \quad (7)$$

where indices j refer to a particular product channel and $k_{tot} = \Sigma k_j$. The ratio of dissociation rates k_j/k_{tot} introduces the coupling between product channels j. The scaling factors $\sigma_{0,j}$ are ideally the same for all product channels although previous experience [20] showed that separate scaling is sometimes needed in order to model data well.

The models represented by Eqs. (5)–(7) are expected to be appropriate for translationally driven ion-molecule reactions [21]. These models have been found to reproduce previous CID and reaction data [8, 10, 12, 22–26]. Uncertainties are calculated considering a series of sources of error: the variation of optimized fit parameters among different data files (2 standard deviations), the range of parameters that allow reasonably good reproduction of data, uncertainties introduced by the ambiguity in the transition state leading to the $C_2H_2S^+$ product, the uncertainty of vibrational frequencies (±10% variation), the uncertainty of the experimentally available time for dissociation (a factor of two variation), and the uncertainty in the absolute energy (±0.05 eV, laboratory frame).

Computational details

To obtain model structures, vibrational frequencies, and energetics for the reactant complex, products, and potentially important intermediates in this system, *ab initio* calculations were carried out using Gaussian 98 [27]. Geometry optimizations and vibrational analyzes were performed at the MP2/6-311+G** level. The vibrational frequencies and rotational constants de-

Table 1. Average thermal energies at 298 K, vibrational frequencies, and rotational constants[a].

Species	$E_{thermal}$[b] (eV)	Frequencies[c] (cm^{-1})	rot const (cm^{-1})	
			1-D	2-D
OCS	0.041 (0.003)	2101, 901, 495 (2)		0.207
OCS^+	0.046 (0.003)	3049, 698, 436, 424		0.195
C_2H_2	0.043 (0.004)	3546, 3455, 1964, 766 (2), 530 (2)		1.162
$C_2H_2^+$	0.039 (0.003)	3405, 3314, 1830, 800, 768, 748, 588		1.144
H_2CCS^+	0.062 (0.004)	3285, 3163, 1536, 1416, 997, 969, 884, 389, 386	9.353	0.192
$c\text{-}C_2H_2S^+$	0.050 (0.004)	3326, 3291, 1613, 1147, 962, 917, 816, 805, 706	1.078	0.353
CO	0.026 (0.001)	2124		1.895
$[OCS \cdot C_2H_2]^+(C_1)$	0.133 (0.010)	3403, 3266, 2185, 1882, 1183, 986, 866, 767, 568, 492, 438, 419, 203, 172, 74	0.270	0.101
$[OCS \cdot C_2H_2]^+(C_s)$	0.133 (0.010)	3479, 3388, 2180, 1936, 826, 793, 789, 690, 614, 449, 425, 405, 253, 99 (2)	0.204	0.088
$[H_2CCS^+ \cdot CO]$	0.175 (0.006)	3289, 3167, 2142, 1526, 1417, 998, 967, 875, 384, 381, 102 (2), 76, 9 (2)	9.358	0.029
$[c\text{-}C_2H_2S^+ \cdot CO]$	0.151 (0.005)	3329, 3295, 2145, 1614, 1143, 955, 909, 823, 807, 704, 106, 91, 79, 10, −23	0.455	0.043
TS_1[d]		3447, 3288, 2205, 1966, 1127, 969, 873, 785, 515, 485, 443, 324, 160, 71	0.257	0.086
TS_2[e]		3402, 3326, 2023, 1791, 837, 826, 757, 664, 511, 483, 433, 416, 142, 75	0.340	0.082
TS_3[f]		3490, 3397, 2182, 1981, 873, 796, 778, 708, 592, 433, 424, 324, 240, 97	0.234	0.078
TS_4[g]		3442, 3287, 2212, 1911, 1191, 949, 787, 784, 584, 526, 447, 418, 193, 148	0.459	0.072
$TS(C_2H_2S)$[h]		3336, 2915, 1828, 1091, 730, 567, 545, 526	2.939	0.193

[a] Obtained from *ab initio* calculations at the MP2/6-311+G** level, see text.
[b] Determined by scaling the frequencies by 0.9676 with uncertainties (in parentheses) representing variations of ±10%.
[c] Degeneracies in parentheses.
[d] Transition state between the $[OCS \cdot C_2H_2]^+$ complexes of C_1 and C_s symmetry, see text.
[e] Transition state between the C_s-symmetry $[OCS \cdot C_2H_2]^+$ complex and the $[c\text{-}C_2H_2S^+ \cdot CO]$ complex.
[f] Transition state between the two optical isomers of the C_s-symmetry $[OCS \cdot C_2H_2]^+$ complex.
[g] Transition state between the two optical isomers of the C_1-symmetry $[OCS \cdot C_2H_2]^+$ complex.
[h] Transition state between H_2CCS^+ and $c\text{-}C_2H_2S^+$.

Table 2. Absolute energies, zero point energies, and relative energies for $C_3H_2OS^+$ species.

System	E(CCD)[a]	E(CCSD)[b]	E(MP2)[c]	E(QCISD)[d]	ZPE[e]	E_{rel}(CCSD)[f]	E_{rel}(QCISD)[g]
	(h)					(eV)	
$C_2H_2^+$	−76.685888	−76.688413	−76.697860	−76.735520	0.025256	1.14	1.25
OCS	−510.683718	−510.689952	−510.772183	−510.815849	0.008798		
C_2H_2	−77.079222	−77.082424	−77.113233	−77.143977	0.025628	1.06	0.96
OCS^+	−510.292352	−510.300707	−510.367011	−510.419688	0.010153		
H_2CCS^+	−474.436216	−474.449493	−474.474879	−474.544250	0.028709	−1.55	−1.46
CO	−113.023185	−113.027130	−113.077817	−113.105993	0.004681	−0.75	−0.65
c-$C_2H_2S^+$	−474.417246	−474.421363	−474.463982	−474.515739	0.029940		
$[OCS \cdot C_2H_2]^+(C_s)$	−587.409637	−587.420583	−587.522582	−587.599535	0.036207	0.05	0.00
$[OCS \cdot C_2H_2]^+(C_1)$	−587.408244	−587.423461	−587.513830	−587.600178	0.037256	0.00	0.01
$[H_2CCS^+ \cdot CO]$	−587.465231	−587.482699	−587.559118	−587.655742	0.034045	−1.70	−1.59
$[c\text{-}C_2H_2S^+ \cdot CO]$	−587.446292	−587.454489	−587.549113	−587.627231	0.035295	−0.90	−0.78
TS_1[h]			−587.513732	−587.599650	0.036717		0.01
TS_2[i]	−587.375161	−587.385756	−587.486269	−587.568575	0.034572	0.95	0.80
TS_3[j]			−587.514089	−587.594551	0.035962		0.13
TS_4[k]	−587.401407	−587.417539	−587.506756	−587.594552	0.037092	0.16	0.16
$TS(C_2H_2S)$[l]			−474.374272	−474.414395	0.025434		1.99
CO	−113.023185	−113.027130	−113.077817	−113.105993	0.004681		

[a] Energy calculated at the CCD/6-31G*//CCD/6-31G* level.
[b] Energy calculated at the CCSD/6-31G*//CCD/6-31G* level.
[c] Energy calculated at the MP2/6-311+G**//MP2/6-311+G** level.
[d] Energy calculated at the QCISD/6-311+G(2d,2p)//MP2/6-311+G** level.
[e] Zero point energy calculated at the MP2/6-311+G** level and scaled by 0.9676.
[f] Relative energies at the CCSD/6-31G*//CCD/6-31G* level, including ZPE at the MP2/6-311+G** level.
[g] Relative energies at the QCISD/6-311+G(2d,2p)//MP2/6-311+G** level, including ZPE at the MP2/6-311+G** level.
[h] Transition state between the $[OCS \cdot C_2H_2]^+$ complexes of C_s and C_1 symmetries.
[i] Transition state between the C_s-symmetry $[OCS \cdot C_2H_2]^+$ and the $[c\text{-}C_2H_2S^+ \cdot CO]$ product complex.
[j] Transition state between the two optical isomers of the C_s-symmetry $[OCS \cdot C_2H_2]^+$ complex.
[k] Transition state between the two optical isomers of the C_1-symmetry $[OCS \cdot C_2H_2]^+$ complex.
[l] Transition state between the H_2CCS^+ and the c-$C_2H_2S^+$ structures.

termined are listed in Table 1. When used to model the data or to calculate thermal energy corrections, the vibrational frequencies are scaled by a factor of 0.9676 designed to bring the calculated values into agreement with experiment [28]. Energetics and zero point energies at this level of theory for the various species considered are given in Table 2. All of the transition states found and discussed below were verified to be first-order transition states by explicit frequency calculations. We also performed reaction path calculations to determine which structures are connected by each of the transition states.

To obtain more accurate energetics, we performed single point energy calculations at a QCISD/6-311+G(2d,2p) level of theory using the MP2/6-311+G** structures. We considered whether to subtract basis set superposition errors (BSSE) from the computed dissociation energies in the full counterpoise approximation [29, 30]. However, such corrections uniformly led to worse agreement with known experimental values and hence are not discussed further. For several species, we also performed geometry optimizations at the CCD/6-31G* level of theory, followed by single point energy calculations at the CCSD/6-31G* level of theory. These results are also provided in Table 2 and discussed further below.

3. Results

CID results

The experimental cross sections for CID with Xe as a function of collision energy are presented in Fig. 1. Results for CID with Ar do not show significant differences. Four products, formed in reactions (8)–(11), are observed.

$$[OCS \cdot C_2H_2]^+ + Xe \rightarrow C_2H_2S^+ + CO + Xe \quad (8)$$

$$\rightarrow OCS^+ + C_2H_2 + Xe \quad (9)$$

$$\rightarrow C_2H_2^+ + OCS + Xe \quad (10)$$

$$\rightarrow S^+ + C_2H_2 + CO + Xe \quad (11)$$

The first to appear and the most important at low energies is the $C_2H_2S^+ + CO$ product channel. It rises rapidly and then declines around 1.2 eV, clearly because of competition with the next product channel, $OCS^+ + C_2H_2$. This latter process has an apparent threshold around 0.5 eV. The $C_2H_2^+ + OCS$ product channel appears around 1.2 eV and rises more slowly to a lower maximum cross section. The least efficient process observed is formation of S^+, which has an apparent threshold around 4.5 eV, consistent with reaction (11), as discussed further below.

All data files show a small (about 1% of the maximum cross section) tail at low energies in the $C_2H_2S^+$ cross section. The tail is not due to multiple collisions in the gas cell because it is not dependent on collision

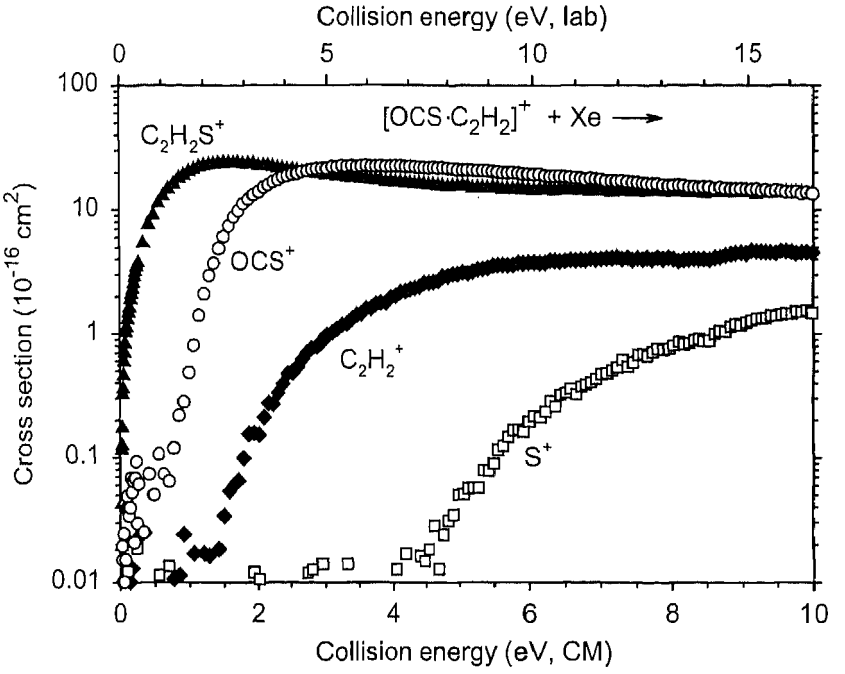

Fig. 1. Product cross sections for collision-induced dissociation of the $[OCS \cdot C_2H_2]^+$ complex with Xe as a function of collision energy in the center-of-mass frame (lower x-axis) and laboratory frame (upper x-axis).

gas pressure. Neither does it appear to be related to insufficient cooling in the ion source because it is not dependent on He flow tube pressure. It also varies in magnitude from data file to data file, which makes modeling difficult because it yields a large spread of threshold values from file to file. One interpretation of this tail is that it results from a second isomer in the reactant ion beam, plausibly $[C_2H_2S \cdot CO]^+$, as discussed below. In order to model the $C_2H_2S^+$ cross section more accurately, we subtracted the average magnitude of the tail (around 1% of the maximum cross section) before analysis. Because of the small magnitude of this tail, the models of these modified files also reproduce the original data files after minor scaling, except at the lowest energies.

The cross section data were analyzed using Eq. (5) and vibrational frequencies and rotational constants provided by the *ab initio* calculations (Table 1). Two possible complexes having C_s and C_1 symmetry (see below) are found, but either set of molecular parameters yields the same results for all levels of modeling. The optimized parameters of Eq. (5) are summarized in Table 3. The fits, presented in Fig. 2, can be seen to reproduce the cross sections well over extended energy ranges.

Table 3. Optimized parameters of the cross section models[a].

Product	σ_0	n	E_0 (eV)	Analysis[b]
$C_2H_2S^+$	24(9)	1.6(0.3)	0.31(0.12)	basic
	24(9)	1.6(0.3)	0.25(0.12)	lifetime[c]
	25(13)	1.4(0.1)	0.34(0.07)	competition[d]
	25(12)	1.5(0.1)	0.32(0.07)	competition[e]
OCS^+	26(9)	1.3(0.3)	1.29(0.09)	basic
	26(9)	1.3(0.3)	1.27(0.09)	lifetime[f]
	38(15)	1.4(0.1)	0.94(0.07)	competition[d]
	31(11)	1.5(0.1)	0.97(0.07)	competition[e]
$C_2H_2^+$	0.8(0.6)	2.1(0.5)	1.52(0.27)	basic
	0.8(0.6)	2.1(0.5)	1.51(0.27)	lifetime[f]
	20(12)	1.4(0.1)	1.22(0.08)	competition[d]
	15(12)	1.5(0.1)	1.22(0.08)	competition[e]
S^+	0.3(0.2)	2.2(0.3)	4.26(0.38)	basic
	0.3(0.2)	2.2(0.3)	3.60(0.38)	lifetime[c]

[a] Uncertainties in parentheses.
[b] "basic" = Eq. (5), "lifetime" = Eq. (6), and "competition" = Eq. (7).
[c] Assuming a tight transition state approximation.
[d] Assuming TS_2 (the transition state between the C_s-symmetry complex and the cyclic products) for the $C_2H_2S^+$ channel and phase space limit transition states for the OCS^+ and $C_2H_2^+$ channels.
[e] Assuming TS_1 (the transition state between the two optical isomers of the C_1-symmetry complex) for the $C_2H_2S^+$ channel and phase space limit transition states for the OCS^+ and $C_2H_2^+$ channels.
[f] Assuming a phase space limit transition state approximation.

To examine possible lifetime effects, the data were also analyzed using the model incorporating RRKM rates, Eq. (6). For the $OCS^+ + C_2H_2$ and $C_2H_2^+ + OCS$ product channels, processes (9) and (10), the most appropriate transition state (TS) is loose and chosen to be in the phase space limit (PSL) [16], such that the molecular parameters needed are simply those of the separated products. As a consequence, the kinetic shifts in these cases, the difference between threshold values obtained using Eqs. (5) and (6) as listed in Table 3, are minor (<0.02 eV).

In the case of the $C_2H_2S^+ + CO$ product channel, process (8), the sulfur transfer reaction requires rearrangement of the atoms over a tight TS. To analyze the cross section for this channel using Eq. (6), we used a very tight TS model to obtain the maximum reasonable kinetic shift. This model assumes that the parameters of the TS are identical to those of the energized molecule minus the vibrational frequency that corresponds to the reaction coordinate, which we assumed is the C–S (in OCS) bond stretch (767 cm^{-1}). A maximum kinetic shift of 0.06 eV is obtained with this

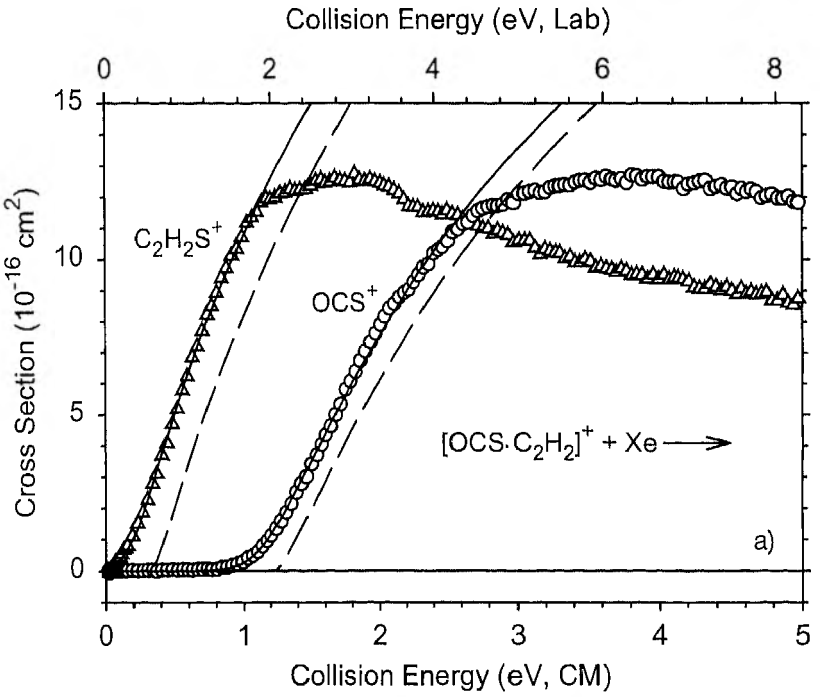

Fig. 2. Cross sections for $C_2H_2S^+$ and OCS^+ (part a) and $C_2H_2^+$ and S^+ (part b) products of collision-induced dissociation of the $[OCS \cdot C_2H_2]^+$ complex with Xe as a function of collision energy in the center-of-mass frame (lower x-axis) and laboratory frame (upper x-axis). Solid lines show the best fits to the data using the model of Eq. (5) with parameters indicated in Table 3, convoluted over the kinetic energy distributions of the reactants. Dashed lines show the same model cross sections in the absence of energy convolution for reactants with an internal temperature of 0 K.

assumption. Similar kinetic shifts (within 0.005 eV) were obtained when any frequency in the range 400–2000 cm^{-1} was removed.

The S^+ channel is most probably a sequential dissociation with a first step forming OCS^+ in reaction (9) and the next step breaking the C–S bond. The TS associated with this latter process is expected to be loose, as for a simple bond rupture without a reverse barrier, but may not be as loose as the PSL. This is because the C–S bond in OCS^+ is a covalent double bond rather than an electrostatic interaction, the situation where PSL applies well. If we again choose a very tight TS by choosing the C–S bond stretch in OCS^+ (767 cm^{-1}) as the reaction coordinate, we obtain a kinetic shift of 0.66 eV. While such a tight TS is not reasonable in this case, it provides an upper limit to the possible kinetic shift. For a PSL loose transition state, the kinetic shift we obtain is 0.21 eV.

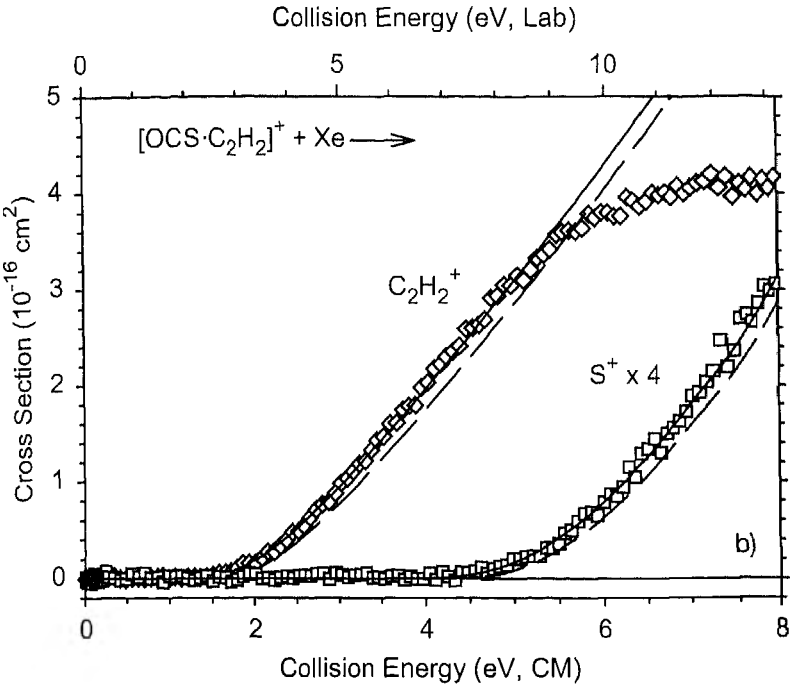

Fig. 2. (Continued).

Finally, we modeled the data using Eq. (7), which takes into account the competition between the product channels. We were able to model the first three product channels ($C_2H_2S^+$, OCS^+ and $C_2H_2^+$) simultaneously by optimizing the fits up to an energy of 2.2 eV. We were not able to include the S^+ channel in the simultaneous analysis because it occurs at much higher energies and is the result of a more complicated sequential dissociation. The optimum parameters of Eq. (7) are listed in Table 3 and the fits presented in Fig. 3. The reproduction of the cross sections for all three channels is very good over the energy range included in the optimization (0 to 2.2 eV) and over about two orders of magnitude. In particular, the model captures the shape of the $C_2H_2S^+$ cross section over a more extended energy range than models (5) or (6), Fig. 2a. Further, there are fewer adjustable parameters because a single value of n is used for all channels. It is worthwhile emphasizing that the implementation of this competitive modeling of ion-molecule reaction cross sections is relatively new [20] and this is the first time that three product channels have been simultaneously modeled.

It is important to note that the reproduction of the data shown in Fig. 3 is obtained by considering at tight TS for the $C_2H_2S^+$ channel and loose

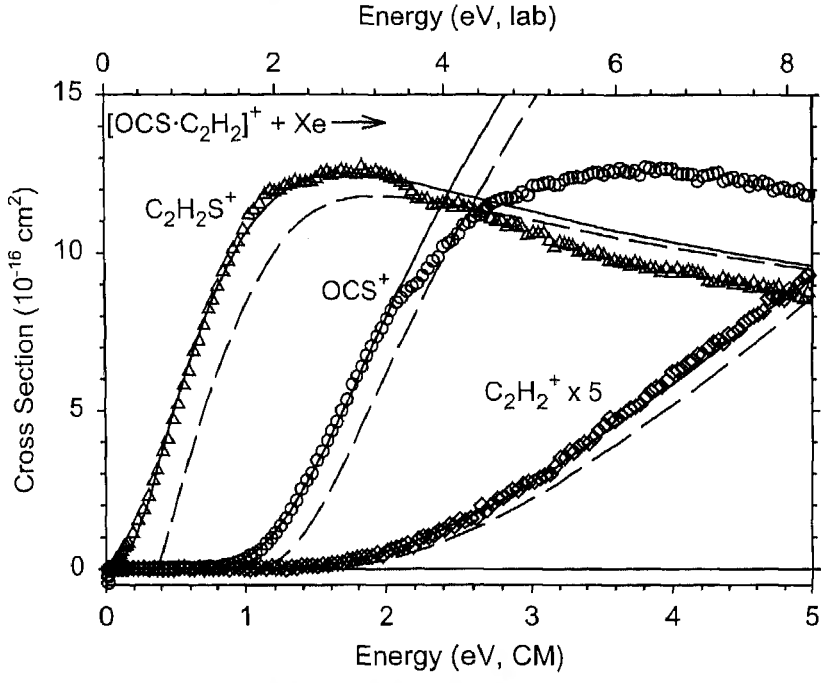

Fig. 3. Cross sections for $C_2H_2S^+$, OCS^+, and $C_2H_2^+$ products of collision-induced dissociation of the $[OCS \cdot C_2H_2]^+$ complex with Xe as a function of collision energy in the center-of-mass frame (lower x-axis) and laboratory frame (upper x-axis). Solid lines show the best fits to the data using the model of Eq. (7) that includes competition, with parameters indicated in Table 3, convoluted over the kinetic energy distributions of the reactants. Dashed lines show the same model cross sections in the absence of energy convolution for reactants with an internal temperature of 0 K.

(PSL) transition states for the other two channels. To ensure that this modeling is not biased by our choice of TS parameters, we considered several transition states for the $C_2H_2S^+$ channel found by *ab initio* calculations, as discussed below. Small differences in the results were obtained, but these are considerably smaller than our experimental uncertainties. TS_2 and TS_3 (described in detail below) were found to represent upper and lower limit to the possible behavior of the true TS, and hence, the final numbers reported for our analysis in Table 3 are averages of the thresholds obtained for these two TSs. No reasonable fit was obtained if all transition states were treated as loose. As shown in Table 3, separate scaling factors $\sigma_{0,j}$ were generally needed in order to reproduce the data with best results. There are no obvious differences in the electronic degeneracies of the various channels and neither mass discrimination nor detection efficiency effects can

consistently account for the difference in scaling factors found. Separate scaling has also been useful in previous applications of the competitive analysis [20] and we continue to investigate the underlying reasons.

Combined competitive and kinetic shifts are given by threshold differences between the basic and competitive analyses (Table 3) obtained using Eqs. (5) and (7). These shifts are small for the leading channel ($C_2H_2S^+$) but significant (about 0.3 eV) for the higher energy channels, reactions (9) and (10). This demonstrates the importance of including competition in the threshold analysis of parallel ion-molecule reactions. The S^+ channel is also expected to have a significant competitive shift, at least as large as the other two higher energy channels. We expect that for systems behaving statistically, competitive shifts should increase as the threshold energy increases. It is also worth noting that thresholds derived from the competitive analysis are more precise than those derived from independent channel analyses, a direct result of the more constrained model of Eq. (7), i.e., the simultaneous analysis of three channels.

Theoretical results

The optimized geometries of the $[OCS \cdot C_2H_2]^+$ complex ion, its CID products, and the relevant transition states were calculated at the MP2/6-311+G** level of theory. The optimized bond lengths and angles for these species are given in Table 4. For the $[OCS \cdot C_2H_2]^+$ complex, we found two stable but nearly isoenergetic structures. In one structure (Fig. 4a) having C_s symmetry, the OCS is nearly linear ($\angle OCS = 177°$) and the sulfur atom interacts with the center of the C−C bond of a slightly distorted C_2H_2 ($\angle HCC = 175°$) unit. The OCS is approximately perpendicular to the plane established by the C_2H_2 and S atom. In the other structure (Fig. 4b) which has no (C_1) symmetry, the sulfur atom is now bonded to only one of the carbon atoms in the C_2H_2 moiety, which is now strongly distorted because the C atom is sp^2 hybridized ($\angle HCC = 131°$) rather than sp hybridized. Again the OCS moiety is perpendicular to the plane established by the C_2H_2 and S atom. This latter structure is the one found by previous calculations of Graul and Bowers [4] at a lower level of theory (HF/6-31+G*).

We also found a transition state that connects the C_s and C_1 complexes, TS_1 (Fig. 4c), by reaction path calculations in which the OCS-C_2H_2 bond length is systematically varied at the MP2/6-31+G* level (a slightly lower level of theory than the geometry optimizations for the stationary points). These reaction path calculations, Fig. 5, show a very shallow well around the C_1 structure, with TS_1 lying only about 0.02 eV above, and the C_s structure being more stable by more than 0.2 eV. Hence, the structure found for TS_1 is very similar to that for the C_1 complex, Table 4. Geometry optimizations of the C_s and C_1 structures as well as of the transition state TS_1 were then performed at the MP2/6-311+G** level. These results gave relative

Table 4. Structural parameters of $C_3H_2OS^+$ species of interest[a].

	R(CO)	R(CS)[b]	R(CS)[c]	R(CC)	R(CH)[d]	∠HCC[d]	∠CSC[e]	∠OCS	∠CSCC
$OCS + C_2H_2^+$	1.170	1.563	–	1.258	1.081	180.0	–	180.0	–
	1.181	*1.562*		*1.258*	*1.082*	*180.0*			
$OCS^+ + C_2H_2$	1.118	1.674	–	1.216	1.065	180.0	–	180.0	–
	1.126	*1.680*		*1.219*	*1.067*	*180.0*			
$H_2CCS^+ + CO$	1.140	–	1.492	1.353	1.088	119.6	–	–	–
	1.150		*1.492*	*1.350*	*1.089*	*119.9*			
$c\text{-}C_2H_2S^+ + CO$	1.140	–	1.764	1.314	1.083	153.2	–	–	–
	1.150		*1.762*	*1.312*	*1.084*	*152.8*			
$[OCS \cdot C_2H_2]^+(C_1)$	1.144	1.634	1.910	1.266	1.083, 1.076	131.2, 155.5	94.0	178.6	96.7
	1.102	*1.679*	*1.838*	*1.314*	*1.073, 1.070*	*126.6, 140.5*	*97.3*	*178.2*	*102.3*
$[OCS \cdot C_2H_2]^+(C_s)$	1.145	1.623	2.649	1.229	1.073	175.1	85.1	177.1	88.8
$[c\text{-}C_2H_2S^- \cdot CO]$	1.137	3.471	1.762	1.315	1.082	152.9, 153.8	119.8	159.8	180.0
$[c\text{-}C_2H_2S^+] \cdot CO]^f(C_{2v})$	1.137	3.328	1.766	1.313	1.082	153.1	158.2	180.0	180.0
$[H_2CCS^+ \cdot CO]$	1.137	3.372	1.493	1.354	1.088	119.6	180.0	180.0	0.0
TS_1[g]	1.145	1.625	1.989	1.248	1.081, 1.073	136.6, 167.4	93.0	178.6	94.1
TS_2[h]	1.149	1.790	2.054	1.256	1.078	165.4, 165.5	118.1	148.4	99.9
TS_3[i]	1.145	1.623	2.724	1.224	1.071	171.6, 177.6	104.7	177.6	0.0
TS_4[j]	1.156	1.630	1.915	1.262	1.081, 1.072	129.5, 158.0	98.8	179.0	0.0
$TS(C_2H_2S)$[k]	–	–	1.806	1.243	1.289, 1.079	65.2, 175.3	177.2	–	–

[a] Bond lengths in angstroms and angles in degrees. Upper values are the present calculations at the MP2/6-311+G** level. Lower values (italics) are previous calculations of Graul and Bowers [4] at the MP2/6-31+G* level, except for $[OCS \cdot C_2H_2]^+$ which was optimized at the HF/6-31+G* level.

[b] Refers to the OC–S bond.

[c] Refers to the S–C_2H_2 bond.

[d] When two numbers are shown, the first refers to the C atom that is closer to the S atom.

[e] Refers to the ∠O-CSC-C angle.

[f] Restricted to C_{2v} symmetry, see text.

[g] Transition state between the $[OCS \cdot C_2H_2]^+$ complexes of C_1 and C_s symmetry.

[h] Transition state between the C_s-symmetric $[OCS \cdot C_2H_2]^+$ and the $[c\text{-}C_2H_2S^- \cdot CO]$ complexes.

[i] Transition state between the two optical isomers of the C_s-symmetric $[OCS \cdot C_2H_2]^+$ complex.

[j] Transition state between the two optical isomers of the C_1-symmetric $[OCS \cdot C_2H_2]^+$ complex.

[k] Transition state between the $c\text{-}C_2H_2S^+$ and the H_2CCS^+ structures.

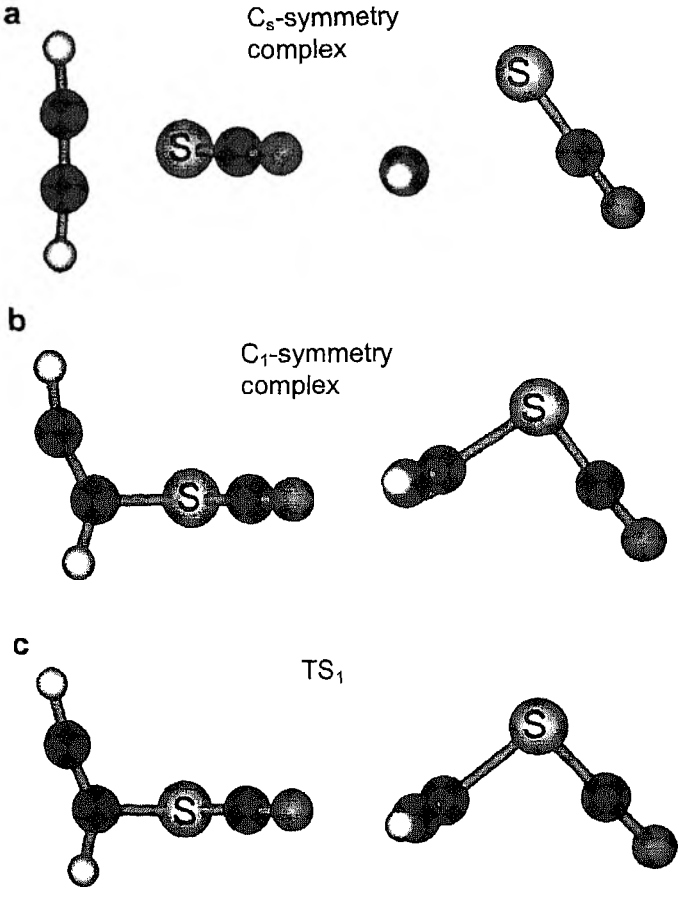

Fig. 4. Optimized structures of the $C_3H_2OS^+$ system in the complex region calculated at the MP2/6-311+G** level of theory: (a) C_s-symmetry $[OCS \cdot C_2H_2]^+$ complex ion; (b) C_1-symmetry $[OCS \cdot C_2H_2]^+$ complex ion; and (c) transition state (TS_1) between the C_1- and the C_s-symmetry complexes. Each structure is shown in two views rotated about the horizontal axis by 90° with respect to each other.

energies that are consistent with the ones from the reaction path calculations at the lower level of theory, Fig. 5. Using these geometries, single point energy calculations at the QCISD/6-311+G(2d,2p) level (Table 2) dramatically lowered the relative energy of the C_1 structure and TS_1. At this level, the C_1 complex is more stable than the C_s complex, but only by about 0.02 eV, while the energy of TS_1 is about the same as that of the C_s structure (within 0.003 eV). These changes clearly point to the idea that multiconfiguration methods are needed to better characterize this potential energy sur-

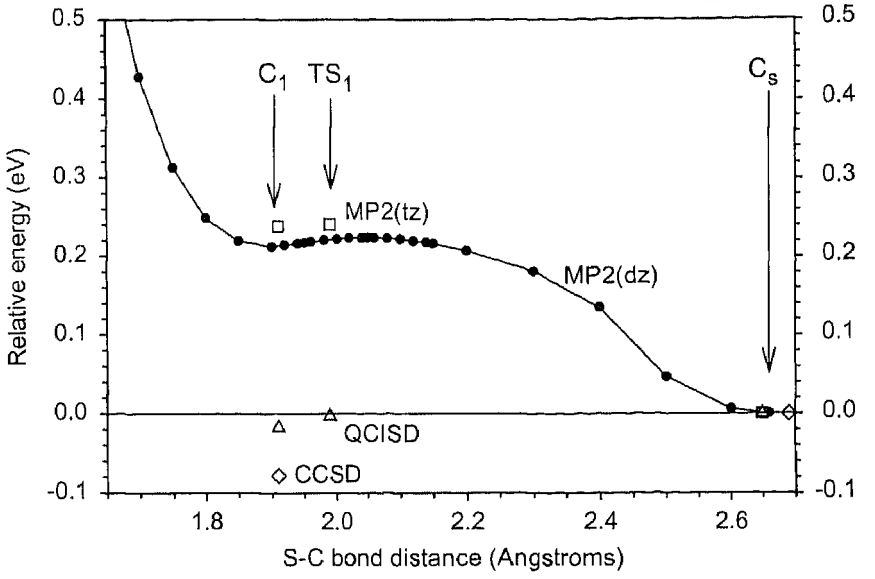

Fig. 5. Reaction path calculations (MP2/6-31+G*) along the $OCS-C_2H_2$ bond coordinate (solid circles), showing the positions of the C_1- and the C_s-symmetry $[OCS \cdot C_2H_2]^+$ complexes, and of the transition state (TS_1) between them. Also shown are results of single point energy calculations for the C_1- and the C_s-symmetry complexes and TS_1 performed at the MP2/6-311+G** level (open squares), QCISD/6-311+G(2d,2p)//MP2/6-311+G** level (open triangles), and CCSD/6-31G*//CCD/6-31G* level (open diamonds). Relative energies are referenced to the energy of the C_s complex for each calculation.

face. Along these lines, we performed another set geometry optimizations using coupled cluster methods. When optimized at the CCD/3-21G level, the C_1 structure collapsed to the C_s-symmetry structure, although for a larger basis set (CCD/6-31G*), both complexes were again found to be local minima. Single point energy calculations using these latter geometries were performed at the CCSD/6-31G* level. These also show that the C_s structure is less stable than the C_1 structure by about 0.08 eV.

None of the relative energies discussed so far include zero point energies. The vibrational energies were calculated for the two complex structures and TS_1 at the MP2/6-311+G** level (Table 1) and are listed in Table 2. When zero point energies are included (a difference of 0.029 eV between the two complexes), we find that the C_s structure is the more stable at all levels of theory except for the CCSD//CCD calculation. For the QCISD//MP2 energies, the difference between the C_s and C_1 complexes is only 0.011 eV and TS_1 has nearly the same energy as the C_1 complex, such that no firm conclusions regarding the global minimum of this complex

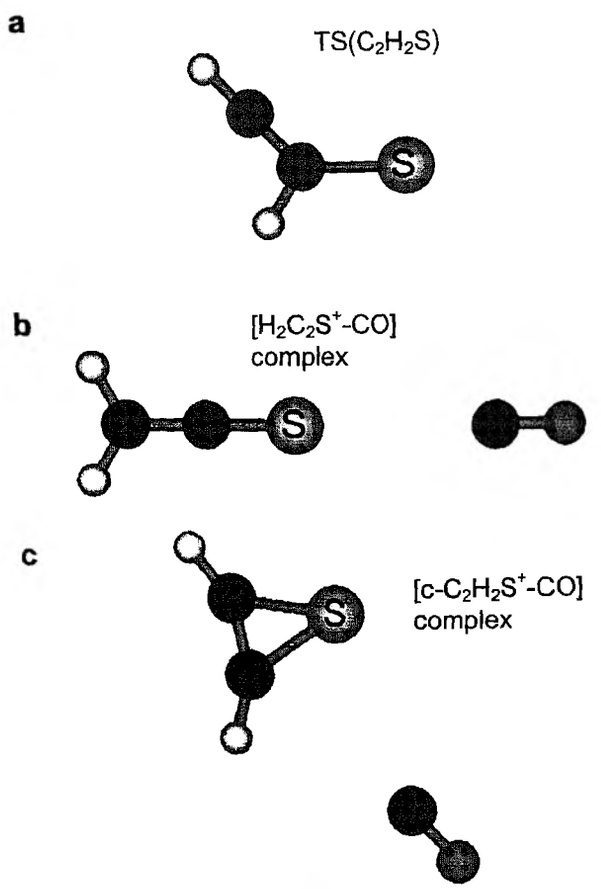

Fig. 6. Optimized structures of the $C_3H_2OS^+$ system in the product region calculated at the MP2/6-311+G** level of theory: (a) TS($C_2H_2S^+$) between the H_2CCS^+ (thioketene) and the c-$C_2H_2S^+$ (cyclic ethylene sulfide) cations; (b) the [$H_2CCS^+ \cdot CO$] product complex; and (c) the [c-$C_2H_2S^+ \cdot CO$] product complex. All structures are planar.

can be made. It seems clear that geometry optimizations performed using multiconfiguration methods are required to characterize this potential energy surface with high accuracy. However, for the purposes of interpreting our experimental results, such calculations are not necessary. On the basis of the QCISD//MP2 results, it seems likely that the relative energy of TS_1 is well below the thermal energy of the $[OCS \cdot C_2H_2]^+$ complex (and certainly the energies required for reaction) such that both geometries are probably in equilibrium and free to interchange upon excitation. It should also be realized that the calculated differences between these complexes are

smaller than our experimental uncertainties such that this structural ambiguity does not change the interpretation of our experimental energies.

We also examined the various structures for the $C_2H_2S^+$ product, thioketene (H_2CCS^+), ethylene sulfide (c-$C_2H_2S^+$), and ethynethiol ($HCCSH^+$). The most stable structure is the thioketene, followed by the ethylene sulfide, about 0.8 eV higher in energy (Table 2). No results for the ethynethiol, which was found as a local minimum by Graul and Bowers at the MP2/6-31+G* level of theory, are included here because it did not converge at the higher level of theory used here. We also found a transition state, TS (C_2H_2S) (Fig. 6a) which connects the thioketene and the ethylene sulfide structures and lies about 2.7 eV higher in energy than the higher energy isomer (ethylene sulfide cation). We calculated structures for the product complexes $[H_2CCS^+ \cdot CO]$ and [c-$C_2H_2S^+ \cdot CO$], presented in Table 4 and Fig. 6b and c. Frequency calculations yielded one negative frequency for the [c-$C_2H_2S^+ \cdot CO$] complex, corresponding to a rotation of the cyclic ethylene sulfide moiety around its C_{2v} axis. The negative frequency, along with several low positive frequencies (Table 1), indicates that the potential energy surface is rather flat. Indeed, a geometry in which the CO is attached to the sulfide along the C_{2v} axis of symmetry was calculated to be only 0.016 eV higher in energy (including zero point energies) than the geometry shown.

A considerable amount of effort was expended in the search for a transition state connecting the $[OCS \cdot C_2H_2]^+$ complex to the $C_2H_2S^+ + CO$ product. Three transition state structures were located. The most plausible one, TS_2, is presented in Fig. 7a and Table 4. The structure is similar to the C_s-symmetry complex, but the OCS moiety is bent ($\angle OCS = 148°$), the OC−S bond length has increased by 0.17 Å, while the S−C_2H_2 bond length has decreased by 0.5 Å. Reaction path calculations started at TS_2 in both directions show that it connects the $[OCS \cdot C_2H_2]^+$ C_s-symmetry and the cyclic [c-$C_2H_2S^+ \cdot CO$] product complexes. Because of this, TS_2 is plausibly the transition state associated with the formation of the $C_2H_2S^+$ product, however, there is a considerable difference between the experimentally observed barrier height to this dissociation (0.33±0.07 eV) and the relative energy of this transition state (0.80 eV), calculated at the QCISD/6-311+G(2d,2p)//MP2/6-311+G** level. This difference may be attributable to the need for multiconfiguration methods, but we also searched for other possible transition states.

Two other transition states were located. The first, TS_3, is presented in Fig. 7b and Table 4. Here, the OCS and C_2H_2 moieties of the C_s-symmetry complex have rotated to lie in the same plane, consistent with motion towards the planar $[H_2CCS^+ \cdot CO]$ or [c-$C_2H_2S^+ \cdot CO$] complexes. Still, a reaction path calculation at the MP2/6-311+G** level of theory reveals that this transition state does not lead to products, but to the other optical isomer of the $[OCS \cdot C_2H_2]^+$ C_s-symmetry complex. (Technically, this is not

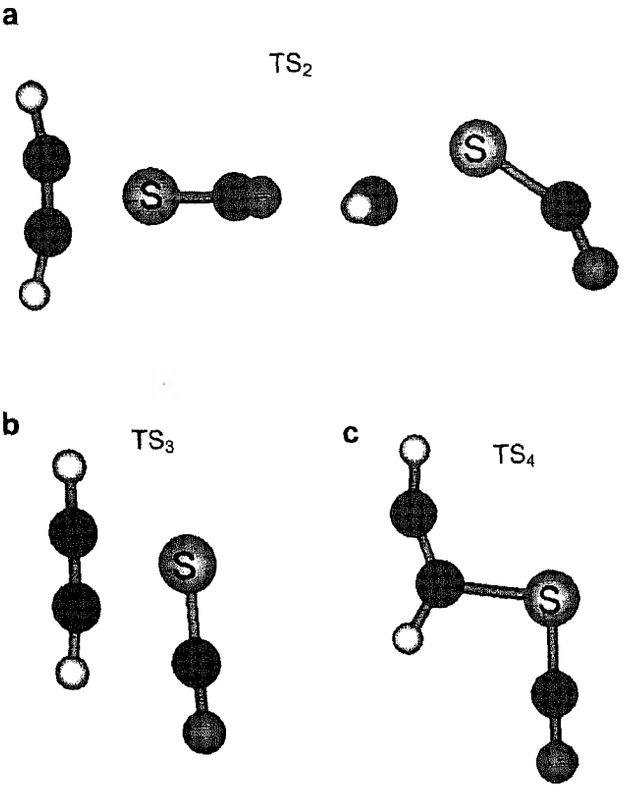

Fig. 7. Optimized structures of transition states in the $C_3H_2OS^+$ system calculated at the MP2/6-311+G** level of theory: (a) TS_2 connecting the C_s-symmetry $[OCS \cdot C_2H_2]^+$ and the $[c\text{-}C_2H_2S^+ \cdot CO]$ product complexes; (b) TS_3 connecting the two optical isomers of the C_s-symmetry $[OCS \cdot C_2H_2]^+$ complex; and (c) TS_4 connecting the two optical isomers of the C_1-symmetry $[OCS \cdot C_2H_2]^+$ complex. For part (a), the structure is shown in two views rotated about the horizontal axis by 90° with respect to each other. For parts (b) and (c), the structures are planar.

an optical isomer because of the symmetry of the C_s complex, however, we use this terminology for convenience and to parallel the situation described below for the C_1-symmetry complex, where there are two optical isomers.) A similar transition state (TS_4) was found to connect the two optical isomers of the C_1-symmetry complex and is presented in Fig. 7c. Because these two transition state structures have planar symmetry, like the products, we also searched for another TS on a pathway starting at one of these structures and leading to one of the product isomers. No other transition state could be located at the level of calculation used here.

Using the structures of all reactant, products, intermediates, and transition states located at the MP2/6-311+G** level, energies were calculated at the MP2/6-311+G** and QCISD/6-311+G(2d,2p) levels of theory, as listed in Table 2. For several cases, using the CCD/6-31G* structures, energies were also calculated at the CCSD/6-31G* level and are presented in Table 2. At the CCSD//CCD level, relative energies are generally comparable (within about 0.1 eV) to the ones at the QCISD//MP2 level. (In both cases, the calculations are referenced to the most stable $[OCS \cdot C_2H_2]^+$ reactant complex so that they correspond to experimental observation.) There are a few differences between the relative energies calculated here (QCISD/6-311+G**) and previously by Graul and Bowers (MP2/6-31+G*). Among them, the most significant are the relative energy between the $C_2H_2^+$ + OCS and OCS^+ + C_2H_2 product asymptotes, 0.29 eV here vs. 0.04 eV previously; the relative energy between the complex and the H_2CCS^+ + CO product, 1.60 eV here vs. 1.32 eV previously; and the relative energies of the two product isomers, $H_2C_2S^+$ and c-$C_2H_2S^+$, 0.81 eV here vs. 0.41 eV previously.

4. Discussion

Thermochemistry

Fig. 8 shows a quantitative reaction coordinate diagram for the $[OCS \cdot C_2H_2]^+$ system derived using the experimental CID results and the *ab initio* calculations at the QCISD/6-311+G(2d,2p)//MP2/6-311+G** level. The thermochemistry [31, 32], available in the literature for the various species of interest is presented in Table 5. The difference between the OCS^+ + C_2H_2 and the $C_2H_2^+$ + OCS asymptotes is equal to the difference in the ionization energies of the two neutral species (0.22 ± 0.01 eV), which are very well known (Table 5). The agreement with our CID value (0.27 ± 0.07 eV) is good, considering the experimental uncertainty. Theoretical values obtained here give a difference of 0.29 eV (QCISD//MP2) and 0.08 eV (CCSD//CCD), while the calculations of Graul and Bowers gave a difference of 0.044 eV. If kinetic shifts and/or competition among channels are not included in our analysis, the energy differences obtained are comparable (Table 3) indicating that these two channels have similar kinetic shifts and are affected similarly by competition with reaction (8).

Another well-known value (Table 5) is the S^+-CO bond dissociation energy (2.28 ± 0.02 eV). The CID threshold determined using Eq. (5) yields an upper limit to this bond energy of <3.34 eV. As discussed above, this is a very conservative limit that does not include kinetic or competitive shifts. These shifts are estimated to exceed 0.3 eV, but cannot be evaluated directly.

The QCISD//MP2 value for the $[OCS \cdot C_2H_2]^+$ complex dissociation energy with respect to the OCS^+ + C_2H_2 asymptote, 0.96 eV, is in very good

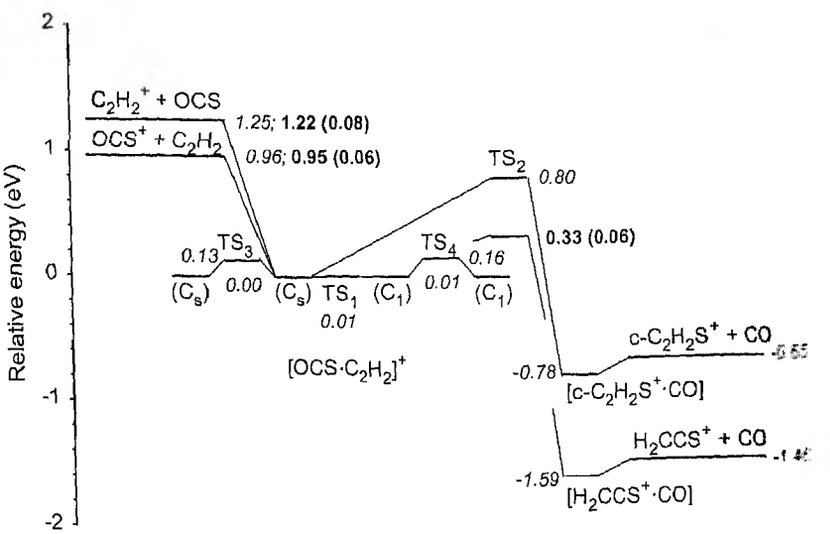

Fig. 8. Potential energy surface for the $[OCS \cdot C_2H_2]^+$ system. Results from experimental CID studies (bold) and *ab initio* calculations at the QCISD/6-311+G(2d,2p)//MP2/6-311+G** level of theory (italics) are indicated.

agreement with the CID value (0.95±0.07 eV), while the CCSD//CCD value is slightly higher, 1.06 eV. All three values agree with the upper limit set by the KERD measurements of Graul and Bowers [4] (<1.15 eV). For dissociation to the $C_2H_2^+$ + OCS asymptote, the QCISD//MP2 value, 1.25 eV, is again in good agreement with the CID value, 1.22±0.08 eV, while the CCSD//CCD value is slightly low, 1.14 eV. All values agree with the upper limit set by the photodissociation experiments of Orlando *et al.* [3], <1.46 eV.

The only heat of formation available in the literature for any of the $C_2H_2S^+$ species concerns the thioketene ion, H_2CCS^+. The heat of formation for this species listed in the compilation of Lias *et al.* [32], 979 kJ/mol, is an uncertain value. Tracing the reference [33] for this value shows that it is not determined experimentally, but was assumed for the purposes of performing RRKM-QET calculations on experimental unimolecular dissociation rate constants. This heat of formation leads to a difference between the $C_2H_2^+$ + OCS and the H_2CCS^+ + CO product asymptotes of 3.44 eV, much higher than the 2.71 eV value derived from our *ab initio* QCISD//MP2 calculations. Clearly, this disagreement is not meaningful.

The CID value for the barrier to the dissociation leading to the $C_2H_2S^+$ product, 0.33±0.07 eV, is consistent with the limit set by Orlando *et al.* [3], >0.15 eV, which was derived considering the thermal energy content of the complex in their PD experiment. The *ab initio* QCISD//MP2 value for this

Table 5. Literature thermochemistry[a].

Molecule	Ionization energy (eV)	Neutral		Ion	
		$\Delta_f H^o$ (kJ/mol, 0 K)	$\Delta_f H^o$ (kJ/mol, 298 K)	$\Delta_f H^o$ (kJ/mol, 0 K)	$\Delta_f H^o$ (kJ/mol, 298 K)
C_2H_2	11.400±0.002[b]	235.755±0.79	226.731±0.79	1335.716±0.81[c]	1326.692±0.81[c]
OCS	11.174±0.002[b]	−138.531±1.05	−138.407±1.05	940.20±1.5[c]	940.32±1.5[c]
H_2CCS	(8.77)[b]		165[b]	(979)[b]	(1011)[b]
CO	14.014[b]	−113.81±0.17	−110.53±0.17	1238.32[b]	1241.59[b]
S	10.360	274.73±0.25	276.98±0.25	1274.31±0.4	1282.29

[a] From Ref. [31], unless otherwise specified.
[b] From Ref. [32]. Parentheses indicate uncertain value, see text.
[c] Calculated from neutral values using ionization energies shown.

transition state (TS_2) is considerably higher, 0.80 eV (and the CCSD//CCD value higher still, 0.95 eV), although we believe that a multiconfiguration level of theory may bring it closer to the experimental value, as discussed above. As noted above, TS_3 and TS_4 might also be considered as the appropriate transition state, although reaction path calculations indicate that neither leads to the $C_2H_2S^+$ product. This is consistent with the observation that both of these transition states lie at much lower energies (0.13 and 0.16 eV, respectively) than the experimental barrier of 0.33±0.07 eV.

Identity of the $C_2H_2S^+$ product

There is an ambiguity about which, if not both, of the two lowest energy isomers of the $C_2H_2S^+$ is the final product of the dissociation. The present CID experiment has no experimental means of resolving this issue. Our calculations were not able to find a path leading from the reactant complex to the lowest isomer (thioketene cation) product channel, while TS_2 provides a pathway to the other isomer, the cyclic ethylene sulfide cation. Also, the very high calculated transition state (2.7 eV) between the two isomers, $TS(C_2H_2S^+)$, excludes the sequential formation of c-$C_2H_2S^+$ followed by isomerization to $H_2C_2S^+$, at least at low energies. Given the weak binding found for CO to the two isomers of $C_2H_2S^+$, 0.13 eV (Table 2), it seems highly unlikely that the presence of CO could affect this TS sufficiently to make formation of thioketene ion a viable pathway for the reaction considered here until very high energies.

The previous experiments of Graul and Bowers [4] also "suggest (but do not mandate)" that only one product is formed, although they state that this is likely to be the more stable of them, the thioketene $(H_2CCS)^+$. They measured the kinetic energy release distribution (KERD) of the $C_2H_2S^+$ + CO product channel. The maximum energy of the KERD allows us to estimate that the top of the barrier is higher than the product asymptote by about 0.9 eV. This can be compared to the sum of the barrier for this reactive channel determined by CID (0.33 eV) and the relative energy for the $C_2H_2S^+$ + CO product asymptote taken from theory. This sum is 1.79 eV for H_2CCS^+ and 0.98 eV for c-$C_2H_2S^+$. The maximum of the KERD data is much higher than the first value, but consistent with the second value. In addition, we have measured axial velocity distributions for this CID product in our guided ion beam instrument [34]. Preliminary analysis of these distributions is most consistent with c-$C_2H_2S^+$ being the product isomer that is formed in CID. Overall, these experimental results and the theoretical results strongly suggest that the most likely product is the higher isomer, c-$C_2H_2S^+$.

Identity of the $C_3H_2OS^+$ complex reactant

Another question that we should address concerns the identity of the reactant complex ion. Is it $[OCS \cdot C_2H_2]^+$, one of the $[C_2H_2S \cdot CO]^+$ isomers,

or a mixture of these? If we produced one of the lower energy isomers, rearrangements over tight transition states would be needed to form the $OCS^+ + C_2H_2$ and $C_2H_2^+ + OCS$ products and a loose, barrierless (simple bond breaking) transition state would lead to the $H_2CCS^+ + CO$ product. In our competitive modeling of CID data, we were not able to obtain a reasonable fit with this combination of transition states, only with the opposite (loose/loose/tight), consistent with the behavior expected for the $[OCS \cdot C_2H_2]^+$ isomer. In addition, Graul and Bowers [4] produced the complex and measured the KERDs of the products of dissociation, finding that there is a reverse barrier to the $C_2H_2S^+$ product channel, so we can conclude that they produced the $[OCS \cdot C_2H_2]^+$ species. Because our ion source conditions are close to theirs, we would expect to produce this isomer, too. However, it is possible that our beam contains some of the lower energy complex $[C_2H_2S \cdot CO]^+$, although its relative abundance should be very small because, according to our calculations, its average internal energy at room temperature (Table 1) equals its well depth (Fig. 8 and Table 1). If this isomer is present in our reactant ion beam, this could account for the tail present in the low energy region of the $C_2H_2S^+$ ion cross section, as described above. This tail would then correspond to the dissociation of this isomer into the $C_2H_2S^+ + CO$ products, with a 0 K threshold of 0.13 eV according to the QCISD//MP2 calculations. The relative magnitude of the tail compared to the maximum $C_2H_2S^+$ ion cross section, approximately 1%, may indicate the relative amount of this lower energy complex present in our beam.

Branching ratios

Product branching ratios as a function of energy are presented in Fig. 9 for the CID experiment. These are compared to results obtained in the previous PD [3] and bimolecular reactions [1, 2]. When comparing branching ratios of the two bimolecular reations with the ones of PD or CID, we must account for the different origins of the energy scales in the four experiments. For the bimolecular reactions, the origin is at the reactant asymptote, while for CID and PD, it is located at the bottom of the potential well for the complex. To compare the ratios on consistent energy scales, we shifted the energy scale for the bimolecular reactions appropriately using values derived in the CID experiment (0.95 eV for $OCS^+ + C_2H_2$ and 1.22 eV for $C_2H_2^+ + OCS$).

The bimolecular reaction experiments have approximately similar trends for the $OCS^+/C_2H_2S^+$ and $C_2H_2^+/C_2H_2S^+$ branching ratios compared with the CID results, but the magnitudes differ. This can be explained by considering the different mechanisms by which products are formed in the two experiments. Differential scattering measurements on the bimolecular reactions [5] reveal that the $C_2H_2S^+$ product is formed via short-range interac-

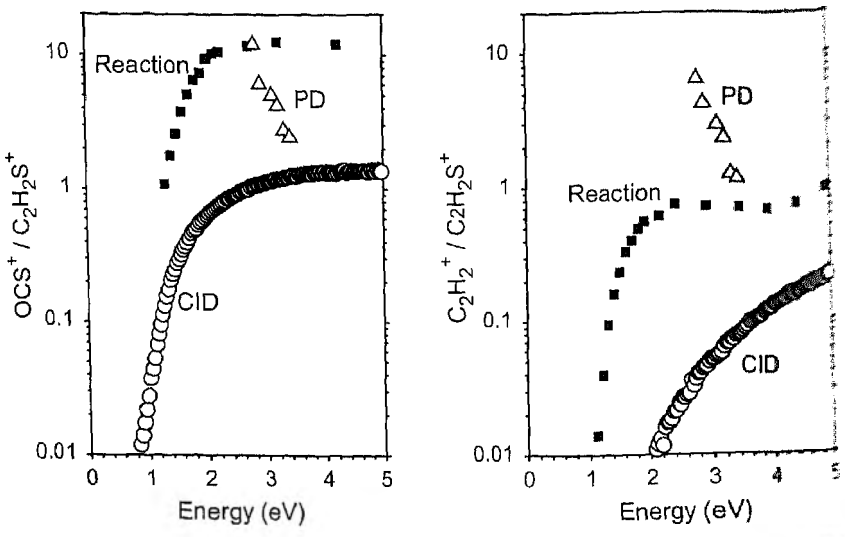

Fig. 9. Product branching ratios as a function of $[OCS \cdot C_2H_2]^+$ excitation energy for the collision-induced dissociation (circles), bimolecular reaction (squares), and photodissociation (triangles) experiments.

tions (complex mediated or rebound) in both reactions (1) and (3), such that this product has relatively small cross sections. In reaction (2), the OCS^+ product is mainly formed by long-range electron transfer, while in reaction (4), the $C_2H_2^+$ product is formed by an impulsive mechanism, both yielding relatively large cross sections. In CID, all the products are formed by similar, short-range interactions between the complex and the collision partner. Therefore, it is reasonable that the CID branching ratios are lower (i.e., yield more $C_2H_2S^+$ product) than the ones for the bimolecular reactions. The $C_2H_2^+/C_2H_2S^+$ branching ratio has a slower rise for CID than for the bimolecular reaction. This can be explained by the fact that, unlike the bimolecular reaction, the $C_2H_2^+$ product formed in CID competes strongly with the OCS^+ product because they both arise from the dissociation of the same energized complex. This competition slows the rise of the $C_2H_2^+$ product cross section.

PD ratios differ considerably from the other two experiments not only in magnitude but also in shape. This is consistent with the belief that PD involves an excited state potential energy surface [3], while the other two experiments explore the ground state surface.

5. Conclusions

The main features of the reaction coordinates of the potential energy surface of the $[OCS \cdot C_2H_2]^+$ system have been quantified by CID experiments. The

products of complex dissociation in the energy range of 0–10 eV are $C_2H_2S^+$, OCS^+, $C_2H_2^+$, and S^+. The complex dissociation energy is 0.95 ± 0.07 eV with respect to the $OCS^+ + C_2H_2$ product channel, 1.22 ± 0.08 eV with respect to the $C_2H_2^+ + OCS$ product channel, and less than 4.26 eV with respect to the $S^+ + CO + C_2H_2$ product channel. The barrier to formation of the $C_2H_2S^+ + CO$ product channel is 0.33 ± 0.07 eV. These energies are determined using simultaneous analysis of the first three product cross sections, including explicit consideration of competition among the channels. The energy dependence of the competition between these three channels has been successfully reproduced using a statistical model with no adjustable parameters. Competition has a significant effect for this system, such that competitive shifts are about 25% of threshold value for the $C_2H_2^+$ and OCS^+ channels and are expected to be significant for S^+, too. These CID thresholds are compatible with all known thermochemical values, within experimental error, and are consistent with limits set by previous photodissociation [3] and KERD measurements [4] on the $[OCS \cdot C_2H_2]^+$ system.

Geometries of the complex ion, products, intermediates, and transition states of interest have been determined by *ab initio* calculations at the MP2/6-311+G** level. The structures are consistent with previous calculations of Graul and Bowers [4] at a lower level of theory, except for the $[OCS \cdot C_2H_2]^+$ complex where we found a second, more symmetric structure at a comparable energy. Energies for the various stationary points on the potential energy surface determined by *ab initio* calculations at a QCISD/6-311+G**//MP2/6-311+G** level agree reasonably well with the ones from CID. The biggest discrepancy is encountered for the transition state leading to the $C_2H_2S^+$ product, where the *ab initio* value is considerably higher. Multiconfiguration methods are probably needed in order to characterize the potential energy surface of this system accurately. These calculations fail to identify a reasonable pathway for production of $H_2C_2S^+$ (thioketene cation), but do find a pathway to form the cyclic ethylene sulfide cation. Previous KERD measurements [3] and preliminary results of present velocity distribution measurements support the hypothesis that the major product formed in the CID of the $[OCS \cdot C_2H_2]^+$ complex is $c\text{-}C_2H_2S^+$.

Acknowledgement

This work is supported by the National Science Foundation, Grant No. CHE-9877162.

References

1. T. M. Orlando, B. Yang, Y. Chui and S. L. Anderson, J. Chem. Phys. **92** (1990) 7356.
2. B. Yang, Y. Chiu and S. L. Anderson, J. Chem. Phys. **94** (1991) 6459.

3. T. M. Orlando, A. Friedmann and J. P. Maier, J. Chem. Phys. **92** (1990) 7365.
4. S. T. Graul and M. T. Bowers, J. Phys. Chem. **95** (1991) 8328.
5. Y. Chiu, H. Fu, J. Huang and S. L. Anderson, J. Chem. Phys. **105** (1996) 3089.
6. K. M. Ervin and P. B. Armentrout, J. Chem. Phys. **83** (1985) 166.
7. R. H. Schultz and P. B. Armentrout, Int. J. Mass Spectrom. Ion Processes **107** (1991) 29.
8. R. H. Schultz, K. C. Crellin and P. B. Armentrout, J. Am. Chem. Soc. **113** (1992) 8590.
9. R. H. Schultz and P. B. Armentrout, J. Chem. Phys. **96** (1992) 1046.
10. F. A. Khan, D. E. Clemmer, R. H. Schultz and P. B. Armentrout, J. Phys. Chem. **97** (1993) 7978.
11. E. R. Fisher, B. L. Kickel and P. B. Armentrout, J. Phys. Chem. **97** (1993) 10204.
12. N. F. Dalleska, K. Honma and P. B. Armentrout, J. Am. Chem. Soc. **115** (1993) 12125.
13. T. S. Beyer and D. F. Swinehart, Commun. Assoc. Comput. Machines **16** (1973) 379.
14. S. E. Stein and B. S. Rabinovitch, J. Chem. Phys. **58** (1973) 2438; Chem. Phys. Lett. **49** (1977) 1883.
15. S. K. Loh, D. A. Hales, L. Lian and P. B. Armentrout, J. Chem. Phys. **90** (1989) 5466.
16. M. T. Rodgers, K. M. Ervin and P. B. Armentrout, J. Chem. Phys. **106** (1997) 4499.
17. R. G. Gilbert and S. C. Smith, *Theory of Unimolecular and Recombination Reactions*, Blackwell Scientific Publications, Oxford (1990).
18. D. G. Truhlar, B. C. Garrett and S. J. Klippenstein, J. Phys. Chem. **100** (1996) 12771.
19. K. A. Holbrook, M. J. Pilling and S. H. Robertson, *Unimolecular Reactions*, 2nd ed., Wiley, New York (1996).
20. M. T. Rodgers and P. B. Armentrout, J. Chem. Phys. **109** (1998) 1787.
21. W. J. Chesnavich and M. T. Bowers, J. Phys. Chem. **83** (1979) 900.
22. M. B. More, E. D. Glendening, D. Ray, D. Feller and P. B. Armentrout, J. Phys. Chem. **100** (1996) 1605.
23. D. Ray, D. Feller, M. B. More, E. D. Glendening and P. B. Armentrout, J. Phys. Chem. **100** (1996) 16116.
24. N. F. Dalleska, K. Honma, L. S. Sunderlin and P. B. Armentrout, J. Am. Chem. Soc. **116** (1994) 3519.
25. L. S. Sunderlin and P. B. Armentrout, Int. J. Mass Spectrom. Ion Processes **94** (1989) 149.
26. P. B. Armentrout, in *Advances in Gas Phase Ion Chemistry*, N. G. Adams, L. M. Babcock, Eds.; JAI Greenwich (1992), Vol. 1, pp. 83–119.
27. Gaussian 98, Revision A.3, M. J. Frisch, G. W. Trucks, H. B. Schlegel, G. E. Scuseria, M. A. Rob, J. R. Cheeseman, V. G. Zakrzewski, J. A. Montgomery, Jr., R. E. Stratmann, J. C. Burant, S. Dapprich, J. M. Millam, A. D. Daniels, K. N. Kudin, M. C. Strain, O. Farkas, J. Tomasi, V. Barone, M. Cossi, R. Cammi, B. Mennucci, C. Pomelli, C. Adamo, S. Clifford, J. Ochterski, G. A. Petersson, P. Y. Ayala, Q. Cui, K. Morokuma, D. K. Malick, A. D. Rabuck, K. Raghavachari, J. B. Foresman, J. Cioslowski, J. V. Ortiz, B. B. Stefanov, G. Liu, A. Liashenko, P. Piskorz, I. Komaromi, R. Gomperts, R. L. Martin, D. J. Fox, T. Keith, M. A. Al-Laham, C. Y. Peng, A. Nanayakkara, C. Gonzalez, M. Challacombe, P. M. W. Gill, B. Johnson, W. Chen, M. W. Wong, J. L. Andres, C. Gonzalez, M. Head-Gordon, E. S. Replogle and J. A. Pople, Gaussian, Inc., Pittsburgh PA (1998).
28. *Exploring Chemistry with Electronic Structure Methods*, 2nd Ed., J. B. Foresman and Æ. Frisch, Gaussian, Pittsburgh (1996).
29. S. F. Boys and R. Bernardi, Mol. Phys. **19** (1970) 553.
30. F. B. van Duijneveldt, J. G. C. M. van Duijneveldt-van de Rijdt and J. H. van Lenthe, Chem. Rev. **94** (1994) 1873.

31. M. W. Chase, Jr., Ed., NIST-JANAF Thermochemical Tables, 4th ed., J. Phys. Chem. Ref. Data, Monograph **9** (1998) 1.
32. S. G. Lias, J. E. Bartmess, J. F. Liebman, R. D. Levin and W. G. Mallard, Gas Phase Ion and Neutral Thermochemistry, J. Phys. Chem. Ref. Data, Vol. 17, Suppl. 1 (1988).
33. J. J. Butler, T. Baer and S. A. Evans, Jr., J. Am. Chem. Soc. **105** (1983) 3451.
34. F. Muntean and P. B. Armentrout, unpublished results.